A Fullerene-platinum Complex for Direct Functional Patterning of Single Metal Atom-embedded Carbon Nanostructures

Dongxu Yang[1,2], Xiangyi Chen[3], Dongsheng He[4], Andreas Frommhold[2], Xiaoqing Shi[5], Stuart Boden[5], Maria A. Lebedeva[6], Olga V. Ershova[6], Richard E. Palmer[4,7], Ziyou Li[4(χ)], Haofei Shi[8], Jianzhi Gao[9]*, Minghu Pan[9]*, Andrei N. Khlobystov[6], Thomas W. Chamberlain[3]*, Alex P. G. Robinson[2]*

[1] State Key Laboratory of Optical Technologies on Nano-Fabrication and Micro-Engineering, Institute of Optics and Electronics, Chinese Academy of Sciences, P.O. Box 350, Chengdu 610209, P. R. China

[2] School of Chemical Engineering, University of Birmingham, Edgbaston, Birmingham B15 2TT, UK

[3] Institute of Process Research and Development, School of Chemistry, University of Leeds, Leeds LS2 9JT, UK

[4] School of Physics and Astronomy, University of Birmingham, Edgbaston, Birmingham B15 2TT, UK

[5] School of Electronics and Computer Science, University of Southampton, Southampton SO17 1BJ, UK

[6] School of Chemistry, University of Nottingham, Nottingham NG7 2RD, UK

[7] College of Engineering, Swansea University, Bay Campus, Fabian Way, Swansea SA1 8EN, UK

[8] Chongqing Institute of Green and Intelligent Technology, Chinese Academy of Sciences, Chongqing 400714, P. R. China

[9] School of Physics and Information Technology, Shaanxi Normal University, Xi'an 710062, China

[(χ)] Prof. Z. Li passed away in December 2020, see also dedication in Note at the end of this article

Keywords: fullerene-platinum complex, functional patterning, resists, electron beam lithography, helium ion beam lithography

ABSTRACT: The development of patterning materials ('resists') at the nanoscale involves two distinct trends – one is towards high sensitivity and resolution for miniaturization, the other aims at functionalization of the resists to realize bottom-up construction of distinct nanoarchitectures. Patterning of carbon nanostructures, a seemingly ideal application for organic functional resists, has been highly reliant on complicated pattern transfer processes due to a lack of patternable precursors. Here we present a fullerene-metal coordination complex as a fabrication material for direct functional patterning of sub-10 nm metal-containing carbon structures. The attachment of one platinum atom per fullerene molecule not only leads to significant improvement of sensitivity and resolution, but also enables stable atomic dispersion of the platinum ions within the carbon matrix, which may gain fundamentally new interest in functional patterning of hierarchical carbon nanostructures.

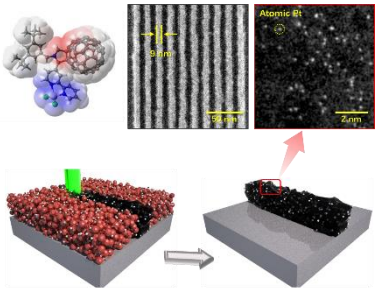

Nanoscale patterning is a fundamental fabrication step in a wide range of advanced solid-state devices such as integrated electronics, chemical and biological sensors, on-chip energy storage units, nanoelectromechanical systems (NEMS), etc.[1-4] Recent developments of lithography techniques have resulted in a boom in device fabrication, and also triggered diversified demands for patterning materials (i.e. resists). In the field of integrated circuit (IC) manufacturing – the most crucial application of nanoscale patterning, stringent targets of resolution and sensitivity are required to push forward miniaturization without losing throughput; whilst in non-electronics applications, functionality enhancement utilizing resist as an active component is often pursued to reduce process complexity.[5-7]

For photolithography in IC manufacturing, resist sensitivity is a key factor that directly determines the throughput. Traditional photoresists employ a chemical amplification (CA) strategy to meet the critical sensitivity requirement.[8] With the continuous shrinkage of feature size, advanced extreme ultraviolet (EUV), electron beam (e-beam) and other charged particle lithographies utilize photons, electrons or ions with energies significantly above the ionization threshold and the exposure is thus driven by radiation chemistry rather than photochemistry.[9] In this case, the energy deposition efficiency is considerably decreased and the exposure sites are more widely scattered. This combined with the random distribution of resist molecules and additional photo-acid diffusion, induce sensitivity and shot noise problems for the traditional polymeric CA resists.[9, 10] One promising solution is utilization of small molecular materials containing high-absorption elements (typically metals), which simultaneously enhances the energy

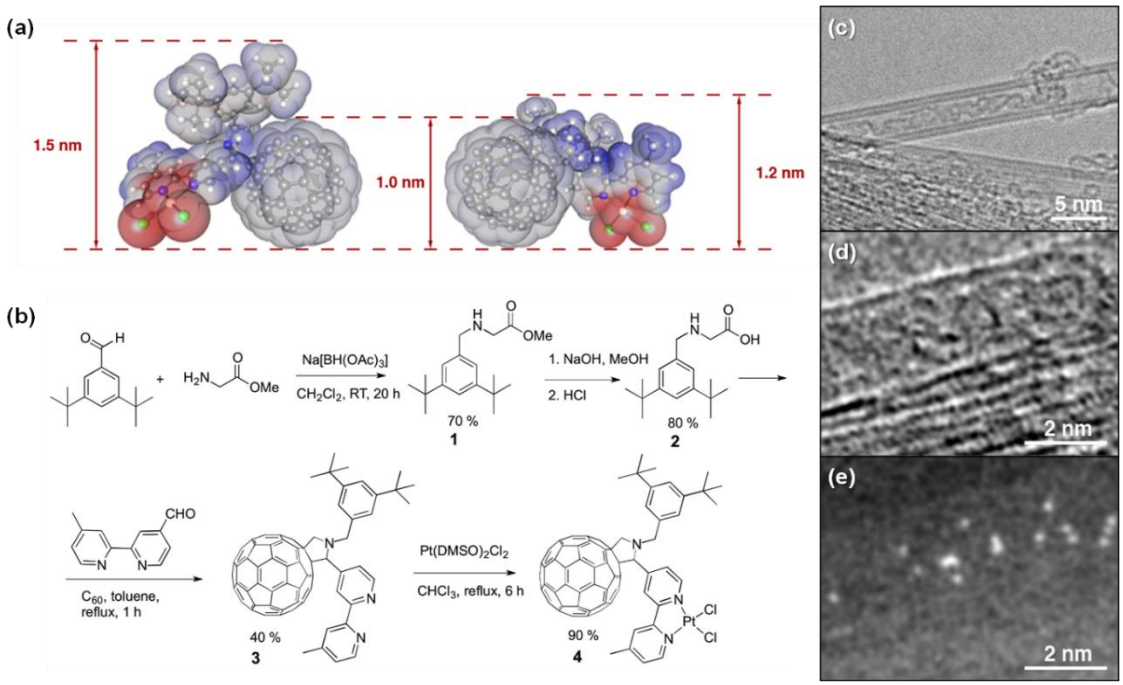

Figure 1. (a) Electrostatic potential surface of the fullerene C_{60}-Bipy-Pt, showing the molecular dimensions; (b) Synthesis of the pyrrolidinofullerene-bipyridine ligand **3** (C_{60}-Bipy), and the Pt complex **4** (C_{60}-Bipy-Pt). (c) shows HRTEM imaging of C_{60}-Bipy-Pt encapsulated within a large diameter DWCNT, forming a pod-like structure; (d) and (e) are simultaneously acquired AC-STEM HAADF and BF images of the corresponding pod-like structure.

deposition efficiency and ultimate resolution. Several metal-based resists such as metal halides,[11] oxides,[12] naphthenates,[13] and metal oxoclusters[14] have been developed, showing promising progress in sensitivity and/or resolution improvement. However, integration of these highly inorganic resists into the semiconductor manufacturing is challenging due to compatibility considerations, such as feasibility of spin-coating, new etching recipe, contamination, etc.[15] Alternatively, complexing metal ions into organic resist systems may be the optimized strategy, but has rarely been reported.[16]

Whilst not common in electronics, functionality enhancement of resists is another favorable direction in diffractive optical elements (DOEs),[17] microelectromechanical systems (MEMS),[18] lithographic insulation patterns (LIPs),[19] all-carbon electronics, [3, 20, 21] etc. This strategy seeks to combine top-down and bottom-up approaches to enable a multiscale structural control. While the lithographic process serves as a typical top-down approach in pattern definition, functionalization of resist materials enables bottom-up tuning of the building blocks, so that the resist pattern can be directly used as active component rather than sacrificial mask.[19, 22] Nevertheless, the development of direct functional patterning is still in its infancy, particularly for the versatile carbon nanostructures. Until now, integration of carbon nanostructures into a miniaturized device typically relies on additional lithography and etch processes, or high-temperature resist carbonization strategy, both of which considerably increase the processing complexity.[18, 23] Although direct writing through focused ion beam (FIB) offers another option, the fabrication speed is much slower than that via lithography routes.[24] Therefore, development of directly patternable materials for functional carbon nanostructure fabrication is highly desirable.[1, 25]

To realize carbon-based functional patterning with high resolution and practical speed, a novel precursor molecule with capability to form amorphous film is essential.[25, 26] Herein we present a fullerene-metal coordination complex, C_{60}-Bipy-Pt, as a patternable functional material for charged particle lithography. We demonstrate that the attachment of one platinum atom per fullerene molecule leads to significant sensitivity and resolution improvement, which offers a new strategy of performance enhancement in organic resists. In addition, atomic dispersion of platinum is observed in the patterned carbon nanostructures with superb stability, which may gain wider interest in functional patterning for applications such as sensors, catalysis, electroless plating, etc.[22, 27]

Synthesis and imaging of C_{60}-Bipy-Pt complex. The molecular structure and synthesis process of the fullerene derivative are shown in Figure 1a and 1b, respectively. The precursor C_{60}-Bipy was prepared via the Prato reaction[28, 29] between the fullerene C_{60}, N-((3,5-di-tert-butylphenyl)methyl)glycine and 4'-methyl-2,2'-bipyridine-4-carboxaldehyde[30] as shown in Figure 1b (compound **3**). Bipyridine is a well-known bidentate chelating ligand that serves to allow facile complexation of the C_{60}-Bipy with a number of transition metals. In this study C_{60}-Bipy-Pt complex (Figure 1b, compound **4**) was formed in a single step via ligand substitution.[29] The detailed synthetic method and compound characterizations by nuclear magnetic resonance (NMR) and Fourier transform infrared (FT-IR) spectroscopy are described in the Methods section and Supporting Information.

To obtain images of dispersed C_{60}-Bipy-Pt molecules, a carbon nanotube encapsulation strategy was employed to form a peapod-like structure, C_{60}-Bipy-Pt@DWCNT (double-walled carbon nanotube). Carbon nanotube serves as an ideal

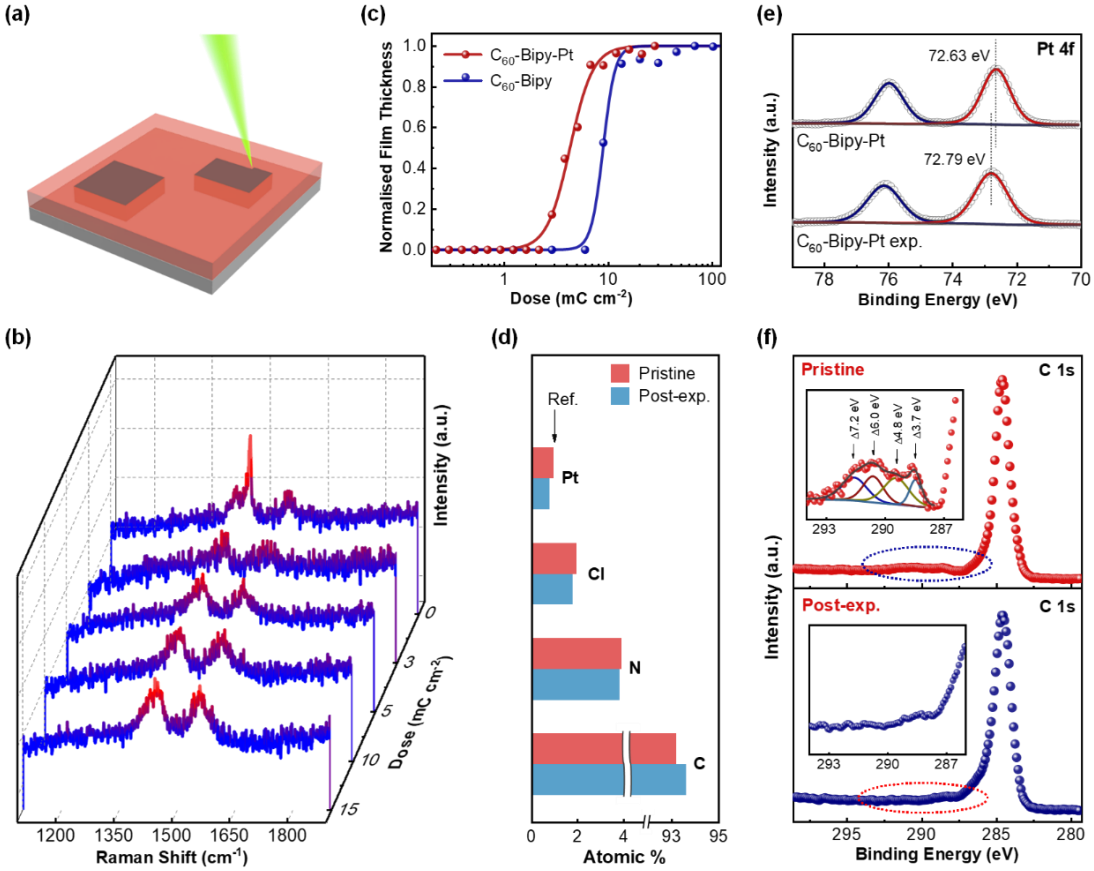

Figure 2. (a) Schematic illustration of the electron beam patterning of the square matrix; (b) Raman spectra of the as-prepared film and lithographically processed (various-dose exposure and development) films of C_{60}-Bipy-Pt; (c) Response curves of C_{60}-Bipy and C_{60}-Bipy-Pt films exposed to electrons at 20 kV and developed in cyclohexanone; (d) Calculated element ratios of C_{60}-Bipy-Pt film before and after 7 mC cm^{-2} electron beam exposure (the position of the arrow mark represents the theoretical value of Pt concentration in the targeted molecule) from XPS spectroscopy; High-resolution XPS spectra of C_{60}-Bipy-Pt film at (e) Pt 4f and (f) C 1s regions. The XPS data is fitted using Gaussian-Lorentzian sum function.

substrate in high-resolution transmission electron microscopy (HRTEM) characterization of single molecules due to their atomically thin sp^2 hybridized carbon framework that can trap and visualize the molecules, and remove any local heating/ionization effects.[31] Density functional theory (DFT) calculation of the van der Waals molecular diameter of C_{60}-Bipy-Pt indicates that only nanotubes with internal diameters greater than ~1.5 nm can accommodate this molecule (Figure 1a).[29] C_{60}-Bipy-Pt@DWCNTs with small (~1.2 nm) and large (~2.2 nm) nanotube internal diameter were separately prepared and imaged. As shown in Figures S1a and S1d, while the narrow nanotubes exhibit an empty interior, filling of fullerene molecule is observed inside the wide DWCNTs, which is in agreement with the DFT modelling and our previous work.[32] Some amorphous carbon residues formed during nanotube fabrication are also observed outside the DWCNTs (Figure 1c). To identify the presence of Pt atoms, imaging with enhanced elemental contrast was performed using high-angle annular dark-field (HAADF) of aberration corrected scanning transmission electron microscopy (AC-STEM).[33, 34] Simultaneously acquired bright field (BF) and HAADF images of C_{60}-Bipy-Pt@DWCNT within a wide nanotube are shown in Figures 1d and 1e, respectively. While some outlines of fullerene cages can be discerned in the BF image, well dispersed Pt atoms are presented as bright dots in the HAADF image due to their high atomic number. The measured size of the bright dots is 0.2 nm, which agrees with the expected size of individual Pt atoms. More images for narrow and wide DWCNT samples are shown in Figure S1 and S2.

Electron-beam-induced changes in C_{60}-Bipy-Pt. To evaluate the response of C_{60}-Bipy and C_{60}-Bipy-Pt to e-beam exposure, the materials were spin-coated onto silicon chips. E-beam sensitivity (at 20 kV) was evaluated through square patterns exposed with various doses and developed in monochlorobenzene (MCB) or cyclohexanone (CYH) (Figure 2a, see Methods and Supplementary Information for more details). The response curves shown in Figure 2c and Figure S3 reveal that upon introduction of platinum, the e-beam sensitivity is improved from 8.9 (10.1) mC cm^{-2} to 4.3 (2.7) mC cm^{-2} in CYH (MCB). This can be attributed to the enhanced secondary electron scattering due to the presence of heavy Pt atoms, which increases the energy deposition efficiency.[10] Whilst slow in comparison to chemically amplified resists, the sensitivity of C_{60}-Bipy-Pt is comparable to the well-known high-resolution resist hydrogen silsesquioxane (HSQ).[35] On the other hand, C_{60}-Bipy-Pt exhibits a higher contrast in CYH development (2.3) than in MCB (1.4), indicating that CYH is a more aggressive developer for this resist, which is beneficial for high-resolution patterning.

Ex-situ Raman measurement was carried out on the patterns with different dosage. As shown in Figure 2b, the Raman

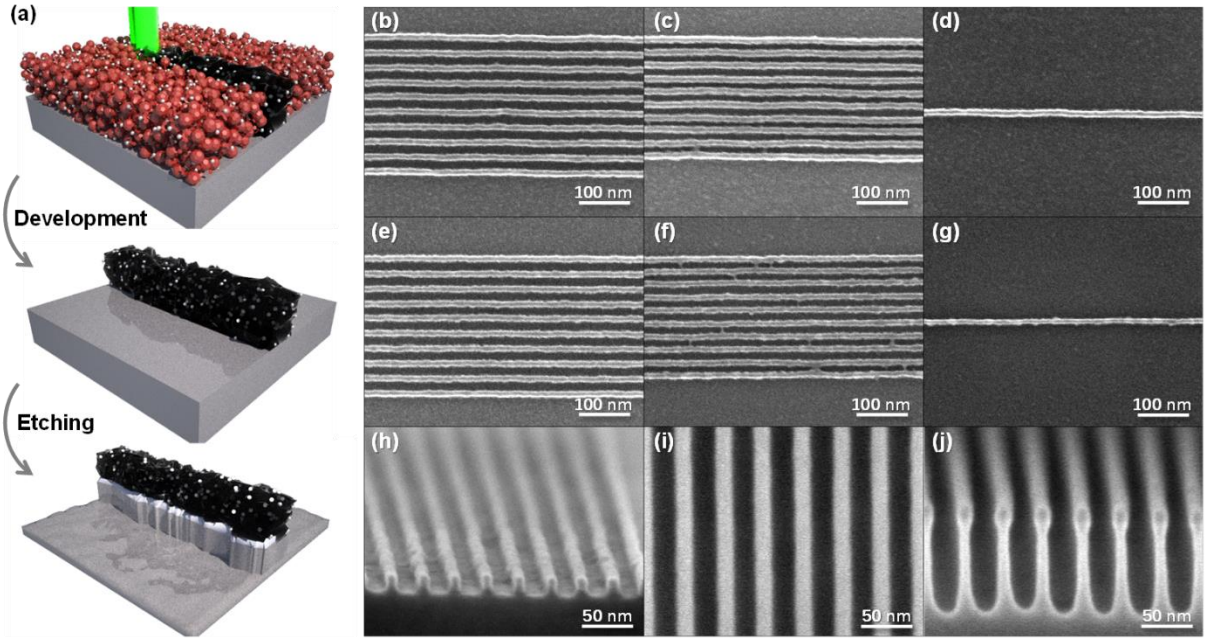

Figure 3. (a) Schematic illustration of the electron beam patterning and etching of the fullerene-metal complex resists; (b) - (d) show SEM micrographs of 32 nm pitch lines and spaces, 28 nm pitch lines and space, and ~12 nm isolated lines, respectively, exposed in the C_{60}-Bipy control material, whilst (e) – (g) show 32 nm and 28 nm pitch lines and spaces, and ~10 nm isolated lines, respectively, in the C_{60}-Bipy-Pt complex. All samples were developed in CYH; (h) The resist profile of C_{60}-Bipy-Pt, seen here at an ~80 °tilt and in 32 nm pitch lines and spaces shows good clearance between the lines and vertical resist walls; (i) ~45 °tilted and (j) ~85 °tilted images of the 40 nm pitch line-space patterns transferred to silicon by ICP etching.

spectrum of pristine C_{60}-Bipy-Pt film exhibits a distinct moiety of the buckminsterfullerene C_{60} with a sharp characteristic peak at 1464 cm^{-1}, corresponding to the double-bond stretching pentagonal pinch mode.[36] The intensity of this peak decreases dramatically upon e-beam exposure at 3 mC cm^{-2} and disappears completely at higher exposure doses, leaving only the D and G bands of the resultant carbon structures. This indicates the fragmentation of C_{60} cages upon e-beam irradiation, followed by formation of an insoluble graphite-like structure, leading to the lithographic behaviour.[37] Notably, the increase of peak intensity at higher dosage is due to the increased residual film thickness. X-ray photoelectron spectroscopy (XPS) characterization was performed to compare the C_{60}-Bipy-Pt films before and after e-beam treatment (Figure S4). The evolution of carbon structure is revealed in the C 1s region of the XPS spectrum (Figure 2f and Figure S5a). The pristine C_{60}-Bipy-Pt film shows a range of π-type shake-up satellites at the high binding energy side of the carbon main line, which matches well with the reported fullerene feature.[38] The exposed film (at 7 mC cm^{-2}), in contrast, does not show these characteristic peaks, again indicating the decomposition of C_{60} cage. In Pt 4f spectrum of C_{60}-Bipy-Pt, the Pt $4f_{7/2}$ peak is located at 72.63 eV, which is in good consistency with literatures for the sub-nm Pt clusters approaching atomic dispersion (Figure 2e).[39-41] The calculated weight ratio of Pt based on peak intensity is 13.0 wt.% (0.9 atom.%), which is in good agreement with the corresponding theoretical value of the proposed molecule (1.0 atom.%), as shown in Figure 2d. After exposure, the binding energy of Pt exhibits a slight positive shift. No metallic Pt(0) is observed in XPS, indicating the absence of the aggregated Pt clusters or particles. A slight shift of binding energy is also observed in the N 1s and Cl 2p region (Figure S5b-c), indicating small amount of charge transfer between Pt and the neighboring atoms, which is likely due to the decomposition of the electrophilic C_{60} cages.[39] Notably, based on the similar concentration and chemical status of Pt, N and Cl before and after exposure, the coordination environment of Pt center should be unaffected. Due to the intrinsic carbon-rich nature of the fullerene derivatives, high plasma etch selectivity between the patterned film and silicon substrate is expected.[37] An etch blanket test (see details in Supplementary Information) was performed using inductively coupled plasma (ICP) with SF_6:CHF_3 as etchant. Both of the materials show high selectivity to silicon under fluorine ICP etching – 13.4 for C_{60}-Bipy and 13.6 for C_{60}-Bipy-Pt, which are significantly better than those of commercial e-beam resists.[37]

Fine patterning by electron and helium ion beam. The e-beam patterning capability of the fullerene derivatives was evaluated through line-and-space (L-S) testing, as schematically illustrated in Figure 3a (see also Figure S6 for the full lithography process flow schematic). Using MCB developer, both the control and the Pt complex are capable of 40 nm pitch dense patterns and ~15.5 nm isolated lines (Figure S7). The resolution was further improved using CYH development (also used in all following tests unless otherwise noted), as predicted by its higher contrast. Clear L-S patterns with 32 nm and 28 nm pitch were obtained in both C_{60}-Bipy (Figure 3b, c) and C_{60}-Bipy-Pt (Figure 3e, f). Images and dosage information for more patterns with larger pitch are shown in Figure S8. Both materials are able to form clearly-resolved L-S pattern down to 30 nm pitch and start showing a slight bridging at pitch 28 nm. As summarized in Table S1, C_{60}-Bipy shows a minimum resolution of >14 nm (~12 nm) in dense (isolated) pattern, while C_{60}-Bipy-Pt is capable of <13 nm (~10 nm) dense (isolated) feature (Figure 3d and 3g). The improved ultimate resolution after Pt incorporation may be attributed to the shot noise reduction resulted from the enhanced

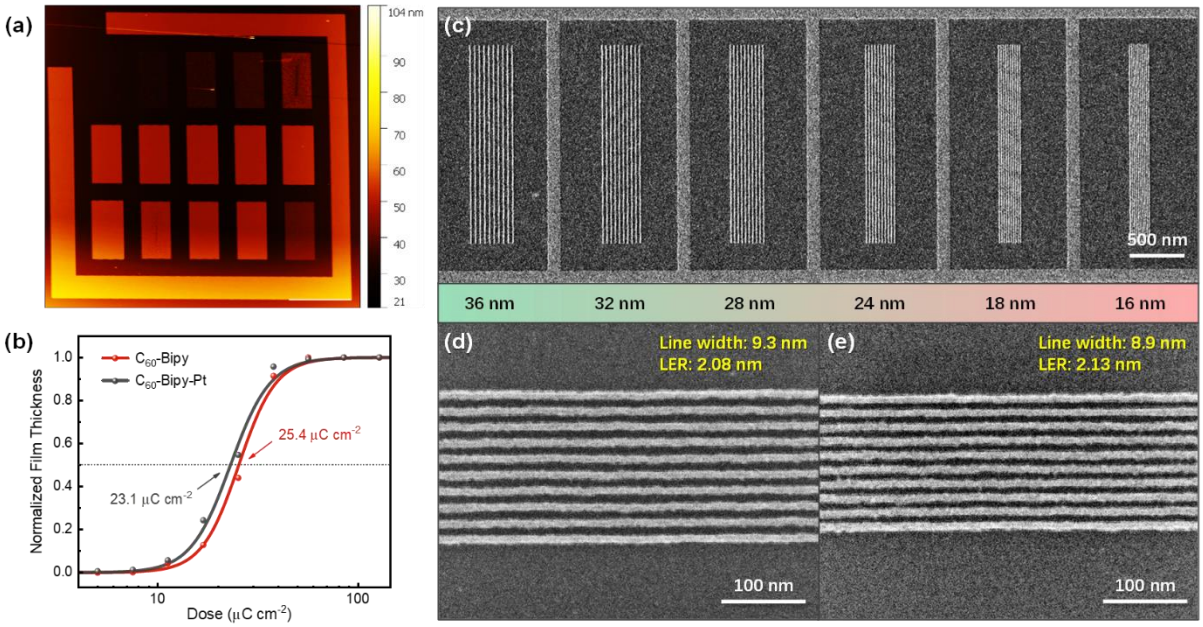

Figure 4. (a) AFM image of an array of the rectangle patterns with various doses exposed by a 30 keV helium ion beam and (b) corresponding response curves for C_{60}-Bipy and C_{60}-Bipy-Pt; (c) Line-space patterns of C_{60}-Bipy-Pt with various pitch sizes from 36 nm to 16 nm, exposed at 62 pC cm^{-1} and imaged by helium ion beam; High-magnification SEM images of (d) 18 nm pitch and (e) 16 nm pitch line-space patterns of C_{60}-Bipy-Pt.

energy deposition.[42] The resolution capability is among the best compared with other advanced e-beam resists under similar exposure conditions.[10, 42, 43] The C_{60}-Bipy-Pt patterns also exhibit near vertical sidewalls (Figure 3h and Figure S9). Combining both high etch selectivity and vertical line profile, high-resolution patterns were successfully transferred from the C_{60}-Bipy-Pt patterns to silicon using fluorine ICP etching (schematically illustrated in Figure 3a). Figures 3i and 3j respectively show the top-down and profile images of the transferred 40 nm pitch lines on silicon with high aspect ratio of ~10. More etched patterns with smaller pitches and isolated features are shown in Figure S10.

Even with remarkable e-beam resolution, the minimum achievable pitch of C_{60}-Bipy-Pt may still be limited by beam spot size and proximity effect. To reduce these influences, the materials were further evaluated by 30 keV helium ion beam (HIB), in which a highly confined energy deposition can be achieved with sub-nanometer beam diameter and negligible backscattering, thus minimizing the proximity effect.[44] Under same process conditions as in the e-beam lithography, an array of 10 μm × 5 μm rectangles were patterned with a dose matrix and probed by atomic force microscope (AFM), as shown in Figure 4a. Notably, an unusual film thickness reduction occurs at large doses due to the etching effect of HIB. This linear contribution was eliminated in the sensitivity evaluation. The calculated sensitivity after fitting are 23.1 μC cm^{-2} for C_{60}-Bipy-Pt and 25.4 μC cm^{-2} for C_{60}-Bipy (Figure 4b). Interestingly, despite being two orders of magnitude faster than the e-beam exposure for both materials, only slight sensitivity improvement was obtained after platinum incorporation. This can be attributed to the high efficiency of secondary electron generation upon HIB exposure even in organic films.[44] Moreover, the small amount of platinum in C_{60}-Bipy-Pt may be insufficient to make notable impact on the scattering properties of the heavy incident ion beam.[45] L-S patterns in a dose-pitch matrix were utilized to evaluate the resolution of C_{60}-Bipy-Pt (~15 nm film thickness), and the obtained patterns were imaged by both helium ion microscopy (HIM) and SEM (Figure S11 and S12). Due to the significantly reduced proximity effect in HIB, the optimized dosage shows no obvious variation at different pitches. At dose 62 pC cm^{-1} (where optimized LER and line width is obtained), line patterns were clearly resolved from 36 nm down to 16 nm pitch - a resolution rarely achieved in other organic resists.[15, 42, 46] Figure 4c displays the HIM image of the above-mentioned patterns. Specifically, a one-to-one line-space pattern of 18 nm pitch was achieved, while an average line width of 8.9 nm was obtained at 16 nm pitch with slight pattern collapse (Figure 4d and 4e). More images for other pitch sizes are shown in Figure S12, further demonstrating the sub-10 nm resolution capability of C_{60}-Bipy-Pt. A small LER of ~2 nm is achieved in all patterns. While the resolution achieved in this work is at the same level with the best results in previous reports, the pattern quality is better than most of the reported materials at similar pattern size.[47]

Atomic resolution imaging of C_{60}-Bipy-Pt film. With the nanoscale patterning capability, it is of interest to investigate the metal distribution within the patterned structures. X-ray (EDX) mapping analysis on a drop-cast film of C_{60}-Bipy-Pt reveals uniform distribution of the key elements (Figure S13). HAADF image exhibits well-scattered dots, of which the size (~0.2 nm) and brightness indicate an atomic dispersion of platinum (Figure 5a and 5b). To test the imaging stability, e-beam scan at 200 kV was applied to the sample in STEM. Close-up views of eight consecutive frames (with additional dose of 167 C cm^{-2} per frame) show no obvious change in the distribution of Pt atoms (Figure S14). A longer continuous scan up to 30 min was also undertaken (Figure S15), where the individual dispersion of Pt atoms still remains, showing a robust stability.

To analyze the resist film under the actual e-beam lithographic conditions (at 30 kV), a relatively thick film (>20 nm) of C_{60}-Bipy-Pt was deposited on a TEM grid with continuous carbon membrane and fabricated with isolated line patterns. Figure S16 and Figure 5c shows the HAADF image of a line

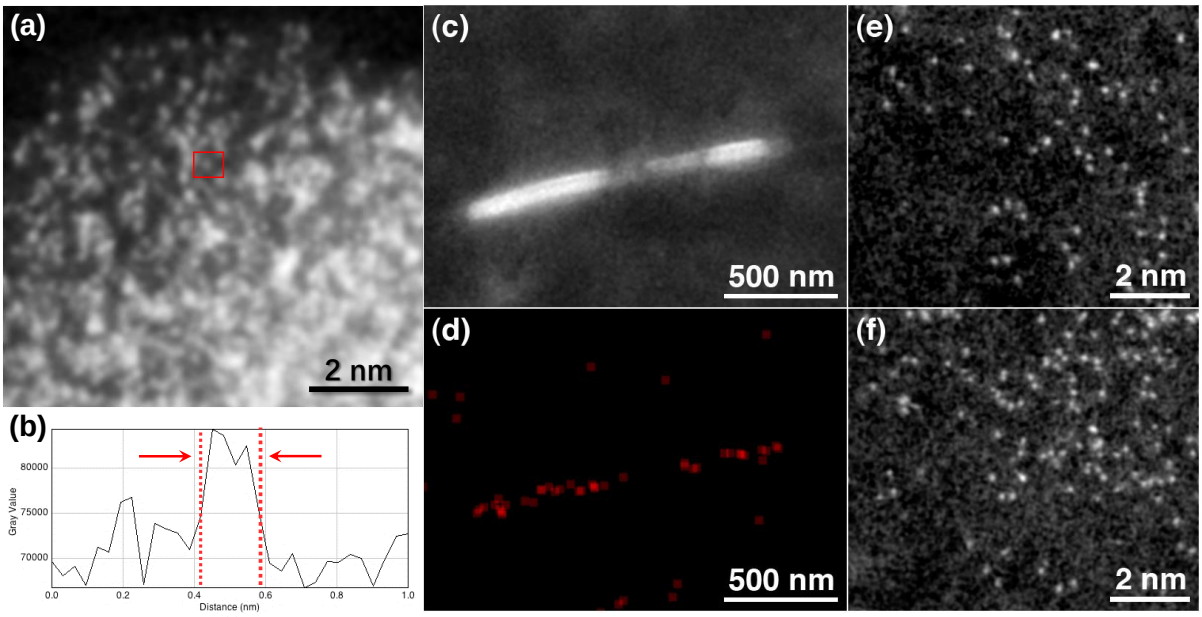

Figure 5. AC-STEM characterization of C_{60}-Bipy-Pt: (a) HAADF image of C_{60}-Bipy-Pt drop-casted on a lacey carbon grid, and (b) the intensity profile of a bright dot region for the Pt element; (c) HAADF image of a patterned line on an amorphous carbon membrane. The discontinuity is ascribed to the unevenness of the resist film and substrate; (d) EDX map of Pt element from (c), confirming that Pt atoms are within the line; (e) HAADF image of a thinner film of C_{60}-Bipy-Pt after open-frame exposure by 30 keV electron beam and (f) shows the same film after subsequent development for 30 s to remove unexposed material.

pattern with high brightness, indicating possible existence of heavy metal. The discontinuity of the line is ascribed to the roughness of both the resist film and the underlying carbon membrane. EDX mapping shows a strong Pt signal confined within the patterned line (Figure 5d). However, the patterned lines are too thick for atomic resolution imaging (a thick film is required for patterning due to the substrate roughness). In order to reveal the effect of the lithography process on the distribution of Pt atoms, flood exposure (at 30 kV) was performed on a significantly thinned film (with low quality), and imaged by STEM before and after development, as shown in Figures 5e and 5f, respectively. It is observed that Pt atoms are individually dispersed within the exposed carbon film and remain so after subsequent development. This is in agreement with the XPS observation that the binding energy in Pt 4f region shows a highly-dispersed state both before and after lithographic process (Figure 2e). More areas from across the sample are shown in Figure S17 (before development) and Figure S18 (after development), further confirming the atomic Pt dispersion.

The presence of stable and well-dispersed heavy metal atoms serves as effective energy absorption centers during the high-energy lithographic irradiation, thus producing increased amount of secondary electrons required for the material transformation.[9, 46] In addition, the enhanced energy deposition is also beneficial for shot noise reduction. As a result, the required dosage can be lowered while the resolution can be potentially improved in charged particle beam patterning. This prototype offers a possible strategy of overall performance enhancement in organic resists for charged particle beam or EUV lithography, where the conventional organic resists generally have a low excitation cross section while the purely inorganic resists have process compatibility issues.[10] Although a non-CA organic resist system with Pt atom complexation is selected in this work, the strategy may be extended to other resist systems with wide choices of heavy metal atoms, particularly for the transition metals that are well-known to form metal-organic coordination, such as Cu, Co, Fe, W, etc.

In summary we have presented a metal-fullerene complex as a new functional patterning material for charged particle lithography, and demonstrated that the incorporation of platinum atoms into the fullerene derivative via complexation leads to a significant enhancement in the electron beam sensitivity without concomitant reduction in the high resolution patterning or etching capabilities. The metal element is found to be atomically distributed within the nanocarbon film and are highly stable against aggregation or leaching even under extreme irradiation doses or aggressive solvents. This work may pave the way for a fundamentally new strategy for both fields of metal-organic resists and carbon functional patterning.

METHODS

Fulleropyrrolidine-Bipyridine preparation and metal complexation: The general synthetic procedure utilized for the preparation of platinum dichloride bipyridine complex, which is described fully in the supplementary methods, involves the complexation reaction between the corresponding bipyridine ligand and $(DMSO)_2PtCl_2$ complex, the latter being prepared in one step from K_2PtCl_4 and DMSO.[48, 49] The novel pyrrolidinofullerene containing bipyridine ligand, **3,** was prepared in 40 % yield *via* the Prato reaction[28] between C_{60} fullerene, bipyridine containing carboxaldehyde[30] and the corresponding N-substituted amino acid, **2**, which contains a 3,5-di-tert-butylbenzyl group to increase the solubility of the target complex. Amino acid **2** was synthesized in two steps *via* the reductive amination of 3,5-di-tert-butyl benzaldehyde with glycine methyl ester to give compound **1** with the subsequent hydrolysis of **1** using sodium hydroxide to give the acid, **2**, in 80 % yield. The fulleropyrrolidino bipyridine platinum dichloride complex, **4**, was prepared in 90 % yield from **3** *via* ligand substitution using $(DMSO)_2PtCl_2$ in which the DMSO ligands

were replaced by the chelating bidentate bipyridine-based ligand.

C_{60}-Bipy-Pt Modelling: Full unconstrained geometry optimization was performed using density functional theory, using Q-Chem and rendered with IQMol, as discussed in the supplementary information.[50]

Preparation of C_{60}-Bipy-Pt@DWCNT: The exohedrally functionalized fullerene, C_{60}-Bipy-Pt, was inserted into nanotubes using the following general method: Purified DWNT (Timesnano, Chengdu Organic Chemicals Co. Ltd.) were annealed in air at 570 ℃ for 30 minutes. A three-fold excess of fullerene was dispersed in toluene (0.2 ml) using an ultrasonic bath to form a super-saturated solution and heated in an inert atmosphere at 80 ℃ for 12 hours. The sample was then filtered (PTFE membrane, pore size = 0.2 μm) before being washed with carbon disulphide (20 ml) to remove any unencapsulated fullerenes and then with methanol (20 ml).

Lithography and SEM Characterization: An XL30 SFEG field emission scanning electron microscope with pattern generator was used for electron beam patterning. After exposure, a dip development in cyclohexanone or monochlorobenzene for 20 s was applied, followed by a rinse in isopropyl alcohol for several seconds. Samples were then dried with nitrogen. For high-resolution patterning a 30 kV acceleration voltage was used with ~50 pA beam current. Single pixel lines were used and dosage is described as a line dose (nC cm^{-1}). The high-resolution structures on silicon substrate were imaged using the same SEM with 5 kV acceleration voltage. Levels have been adjusted to enhance contrast, and images cropped for clarity but they are otherwise unprocessed (raw images are shown in the supplementary information). Helium ion beam lithography (HIBL) was performed by in an Orion™ Plus helium ion microscope (Carl Zeiss) in the University of Southampton. The beam energy was 30 keV for both patterning and imaging. Area patterns and line-space patterns on silicon were etched with an Oxford Instruments PlasmaPro NGP80 tool using an inductively coupled plasma (ICP) as discussed in the Supplementary information.

ASSOCIATED CONTENT

Supporting Information. This material is available free of charge via the Internet at http://pubs.acs.org.

AUTHOR INFORMATION

Corresponding Author

* Thomas W. Chamberlain - Institute of Process Research and Development, School of Chemistry, University of Leeds, Leeds LS2 9JT, UK; E-mail: t.w.chamberlain@leeds.ac.uk

* Alex P. G. Robinson - School of Chemical Engineering, University of Birmingham, Edgbaston, Birmingham B15 2TT, UK; Email: a.p.g.robinson@bham.ac.uk

* Jianzhi Gao - School of Physics and Information Technology, Shaanxi Normal University, Xi'an 710062, China; Email: jianzhigao@snnu.edu.cn

* Minghu Pan - School of Physics and Information Technology, Shaanxi Normal University, Xi'an 710062, China; Email: minghupan@snnu.edu.cn

Notes

This manuscript is dedicated to the memory of our co-author Dr Ziyou Li, a fine scientist and a good friend, who sadly passed away shortly before this paper was submitted.

SUPPORTING INFORMATION

Detailed methods for material synthesis and modeling, sample preparation, sensitivity and contrast evaluation, and plasma etching; additional HRTEM and STEM images; additional XPS spectra; schematics for lithography and etching processes; additional SEM images for resist patterns and etched patterns; EDX elemental mapping data, etc.

ACKNOWLEDGMENT

The authors acknowledge support from the Engineering and Physical Sciences Research Council, and the European Research Council. The STEM instrument, Oxford Instruments PlasmaPro NGP80 Inductively Coupled Plasma etching system and Disco DAD 321 wafer dicer used in this research were obtained through Birmingham Science City: Creating and Characterizing Next Generation Advanced Materials, with support from Advantage West Midlands and part funded by the European Regional Development Fund. DXY and DSH thank the University of Birmingham and China Scholarship Council (CSC) for support.

REFERENCES

(1) Tu, M, Xia, B, Kravchenko, DE, Tietze, ML, Cruz, AJ, Stassen, I, Hauffman, T, Teyssandier, J, De Feyter, S, Wang, Z, Fischer, RA, Marmiroli, B, Amenitsch, H, Torvisco, A, Vel ásquez-Hern ández, MDJ, Falcaro, P, Ameloot, R, Direct X-Ray and Electron-Beam Lithography of Halogenated Zeolitic Imidazolate Frameworks. *Nat Mater* **2021**, *20*, 93-99.
(2) He, Q, Zhang, H, Nanoscale Patterning Hots Up. *Nat Electron* **2019**, *2*, 13-14.
(3) Qiu, C, Zhang, Z, Xiao, M, Yang, Y, Zhong, D, Peng, LM, Scaling Carbon Nanotube Complementary Transistors to 5-nm Gate Lengths. *Science* **2017**, *355*, 271-276.
(4) Chen, H, Zhang, W, Li, M, He, G, Guo, X, Interface Engineering in Organic Field-Effect Transistors: Principles, Applications, and Perspectives. *Chem Rev* **2020**, *120*, 2879-2949.
(5) Stassen, I, Styles, M, Grenci, G, Gorp, HV, Vanderlinden, W, Feyter, SD, Falcaro, P, Vos, DD, Vereecken, P, Ameloot, R, Chemical Vapour Deposition of Zeolitic Imidazolate Framework Thin Films. *Nat Mater* **2016**, *15*, 304-310.
(6) Palmer, RE, Robinson, APG, Guo, Q, How Nanoscience Translates Into Technology: The Case of Self-Assembled Monolayers, Electron-Beam Writing, and Carbon Nanomembranes. *ACS Nano* **2013**, *7*, 6416-6421.
(7) Qin, D, Xia, Y, Whitesides, GM, Soft Lithography for Micro- and Nanoscale Patterning. *Nat Protoc* **2010**, *5*, 491-502.
(8) MacDonald, SA, Willson, CG, Frechet, J, Chemical Amplification in High-Resolution Imaging-Systems. *Acc Chem Res* **1994**, *27*, 151-158.
(9) Kozawa, T, Radiation Chemistry in Chemically Amplified Resists. *Jpn J Appl Phys* **2010**, *49*, 030001-030001-19.
(10) Lawson, R, Frommhold, A, Yang, D, Robinson, A, Negative-Tone Organic Molecular Resists. In *Materials and Processes for Next Generation Lithography*, A. Robinson and R. Lawson Eds, Elsevier **2016**, p 223.
(11) Muray, A, Radiolysis and Resolution Limits of Inorganic Halide Resists. *J Vac Sci Technol B* **1985**, *3*, 367-373.
(12) Krysak, M, Trikeriotis, M, Schwartz, E, Lafferty, N, Xie, P, Smith, B, Zimmerman, P, Montgomery, W, Giannelis, E, Ober, CK, Development of an Inorganic Nanoparticle Photoresist for EUV, E-Beam, and 193 nm Lithography. *Proc. SPIE* **2011**, *7972*, 79721C.
(13) Nedelcu, M, Saifullah, MSM, Hasko, DG, Jang, A, Anderson, D, Huck, WTS, Jones, GAC, Welland, ME, Kang, DJ, Steiner, U, Fabrication of Sub-10 nm Metallic Lines of Low Line-Width Roughness by Hydrogen Reduction of Patterned Metal-Organic Materials. *Adv Funct Mater* **2010**, *20*, 2317-2323.

(14) Wu, L, Bespalov, I, Witte, K, Lugier, O, Haitjema, J, Vockenhuber, M, Ekinci, Y, Watts, B, Brouwer, AM, Castellanos, S, Unravelling the Effect of Fluorinated Ligands in Hybrid EUV Photoresists by X-Ray Spectroscopy. *J Mater Chem C* **2020**, *8*, 14757-14765.
(15) Li, L, Liu, X, Pal, S, Wang, S, Ober, CK, Giannelis, EP, Extreme Ultraviolet Resist Materials for Sub-7 nm Patterning. *Chem Soc Rev* **2017**, *46*, 4855-4866.
(16) Haller, I, Feder, R, Hatzakis, M, Spiller, E, Copolymers of Methyl Methacrylate and Methacrylic Acid and their Metal Salts as Radiation Sensitive Resists. *J Electrochem Soc* **1979**, *126*, 154-161.
(17) Pan, J, Rong, Z, Wang, Y, Cho, H, Coropceanu, I, Wu, H, Talapin, DV, Direct Optical Lithography of Colloidal Metal Oxide Nanomaterials for Diffractive Optical Elements with 2π Phase Control. *J Am Chem Soc* **2021**, *143*, 2372-2383.
(18) Wang, C, Madou, M, From Mems to Nems with Carbon. *Biosens Bioelectron* **2005**, *20*, 2181-2187.
(19) Chen, M, Lai, C, Chen, H, Lin, Y, Huang, K, Lin, C, Hsiao, H, Liu, L, Chen, C, Preparation of Photosensitive Polyimides (PSPIs) and their Feasible Evaluation for Lithographic Insulation Patterns (LIPs) of Integrated Circuits (ICs) without Negative Photoresists. *Mat Sci Semicon Proc* **2018**, *88*, 132-138.
(20) Tan, Z, Zhang, D, Tian, H, Wu, Q, Hou, S, Pi, J, Sadeghi, H, Tang, Z, Yang, Y, Liu, J, Tan, Y, Chen, Z, Shi, J, Xiao, Z, Lambert, C, Xie, S, Hong, W, Atomically Defined Angstrom-Scale All-Carbon Junctions. *Nat Commun* **2019**, *10*, 1748-1748.
(21) Franklin, AD, The Road to Carbon Nanotube Transistors. *Nature* **2013**, *498*, 443-444.
(22) Liu, J, Li, M, Yang, Y, Xu, L, Lin, J, Hong, W, Chen, X, Metal Conductive Surface Patterning on Photoactive Polyimide. *Adv Funct Mater* **2017**, *27*, 1701674.
(23) Qi, D, Liu, Y, Liu, Z, Zhang, L, Chen, X, Design of Architectures and Materials in in-Plane Micro-Supercapacitors: Current Status and Future Challenges. *Adv Mater* **2017**, *29*, 1602802.
(24) Abbas, AN, Liu, G, Liu, B, Zhang, L, Liu, H, Ohlberg, D, Wu, W, Zhou, C, Patterning, Characterization, and Chemical Sensing Applications of Graphene Nanoribbon Arrays Down to 5 nm Using Helium Ion Beam Lithography. *ACS Nano* **2014**, *8*, 1538-1546.
(25) Gibbons, FP, Manickam, M, Preece, JA, Palmer, RE, Robinson, APG, Direct Electron-Beam Writing of Highly Conductive Wires in Functionalized Fullerene Films. *Small* **2009**, *5*, 2750-2755.
(26) Yang, DX, Frommhold, A, Xue, X, Palmer, RE, Robinson, APG, Chemically Amplified Phenolic Fullerene Electron Beam Resist. *J Mater Chem C* **2014**, *2*, 1505.
(27) Zhang, J, Feng, J, Jia, L, Zhang, H, Zhang, G, Sun, S, Zhou, T, Laser-Induced Selective Metallization on Polymer Substrates Using Organocopper for Portable Electronics. *ACS Appl Mater Interfaces* **2019**, *11*, 13714-13723.
(28) Maggni, M, Scorrano, G, Prato, M, Addition of Azomethine Ylides to C-60 - Synthesis, Characterization, and Functionalization of Fullerene Pyrrolidines. *J Am Chem Soc* **1993**, *115*, 9798-9799.
(29) Lebedeva, MA, Chamberlain, TW, Scattergood, PA, Delor, M, Sazanovich, IV, Davies, ES, Suyetin, M, Besley, E, Schröder, M, Weinstein, JA, Khlobystov, AN, Stabilising the Lowest Energy Charge-Separated State in a {Metal Chromophore – Fullerene} Assembly: A Tuneable Panchromatic Absorbing Donor–Acceptor Triad. *Chem Sci* **2016**, *7*, 5908-5921.
(30) Strouse, GF, Schoonover, JR, Duesing, R, Boyde, S, Jones, WE, Meyer, TJ, Influence of Electronic Delocalization in Metal-to-Ligand Charge-Transfer Excited-States. *Inorg Chem* **1995**, *34*, 473-487.
(31) Gimenez-Lopez, MC, Chuvilin, A, Kaiser, U, Khlobystov, AN, Functionalised Endohedral Fullerenes in Single-Walled Carbon Nanotubes. *Chem Commun* **2011**, *47*, 2116-8.
(32) Chamberlain, TW, Pfeiffer, R, Howells, J, Peterlik, H, Kuzmany, H, Krautler, B, Da, RT, Melle-Franco, M, Zerbetto, F, Milic, D, Khlobystov, AN, Engineering Molecular Chains in Carbon Nanotubes. *Nanoscale* **2012**, *4*, 7540-8.
(33) Nicholls, RJ, Sader, K, Warner, JH, Plant, SR, Porfyrakis, K, Nellist, PD, Briggs, GAD, Cockayne, DJH, Direct Imaging and Chemical Identification of the Encapsulated Metal Atoms in Bimetallic Endofullerene Peapods. *ACS Nano* **2010**, *4*, 3943-3948.
(34) Allen, JE, Hemesath, ER, Perea, DE, Lensch-Falk, JL, Li, ZY, Yin, F, Gass, MH, Wang, P, Bleloch, AL, Palmer, RE, Lauhon, LJ, High-Resolution Detection of Au Catalyst Atoms in Si Nanowires. *Nat Nanotechnol* **2008**, *3*, 168-173.
(35) Manfrinato, VR, Zhang, L, Su, D, Duan, H, Hobbs, RG, Stach, EA, Berggren, KK, Resolution Limits of Electron-Beam Lithography Toward the Atomic Scale. *Nano Lett* **2013**, *13*, 1555-1558.
(36) Bethune, DS, Meijer, G, Tang, WC, Rosen, HJ, The Vibrational Raman Spectra of Purified Solid Films of C60 and C70. *Chem Phys Lett* **1990**, *174*, 219-222.
(37) Robinson, APG, Palmer, RE, Tada, T, Kanayama, T, Shelley, EJ, Philp, D, Preece, JA, Exposure Mechanism of Fullerene Derivative Electron Beam Resists. *Chem Phys Lett* **1999**, *312*, 469-474.
(38) Leiro, JA, Heinonen, MH, Laiho, T, Batirev, IG, Core-Level Xps Spectra of Fullerene, Highly Oriented Pyrolitic Graphite, and Glassy Carbon. *J Electron Spectrosc* **2003**, *128*, 205-213.
(39) Li, D, Li, X, Chen, S, Yang, H, Wang, C, Wu, C, Haleem, YA, Duan, S, Lu, J, Ge, B, Ajayan, PM, Luo, Y, Jiang, J, Song, L, Atomically Dispersed Platinum Supported on Curved Carbon Supports for Efficient Electrocatalytic Hydrogen Evolution. *Nat Energy* **2019**, *4*, 512-518.
(40) Jia, L, Bulushev, DA, Podyacheva, OY, Boronin, AI, Kibis, LS, Gerasimov, EY, Beloshapkin, S, Seryak, IA, Ismagilov, ZR, Ross, JRH, Pt Nanoclusters Stabilized by N-Doped Carbon Nanofibers for Hydrogen Production From Formic Acid. *J Catal* **2013**, *307*, 94-102.
(41) Kim, Y, Ohshima, K, Higashimine, K, Uruga, T, Takata, M, Suematsu, H, Mitani, T, Fine Size Control of Platinum on Carbon Nanotubes from Single Atoms to Clusters. *Angew Chem Int Ed* **2006**, *45*, 407-411.
(42) D, PP, W, HC, Claudia, L, Steve, L, Marcus, K, Tzvetan, I, Ahmad, A, W, RI, Xiaoqing, S, A, BS, Robinson, APG, Dongxu, Y, Sangeetha, H, Marijke, S, Ejaz, H, Charged Particle Single Nanometre Manufacturing. *Beilstein J Nanotech* **2018**, *9*, 2855-2882.
(43) Gangnaik, AS, Georgiev, YM, Holmes, JD, New Generation Electron Beam Resists: A Review. *Chem Mater* **2017**, *29*, 1898-1917.
(44) Lewis, SM, Hunt, MS, DeRose, GA, Alty, HR, Li, J, Wertheim, A, De Rose, L, Timco, GA, Scherer, A, Yeates, SG, Winpenny, REP, Plasma-Etched Pattern Transfer of Sub-10 nm Structures Using a Metal–Organic Resist and Helium Ion Beam Lithography. *Nano Lett* **2019**, *19*, 6043-6048.
(45) Joshi-Imre, A, Bauerdick, S, Direct-Write Ion Beam Lithography. *J Nanotech* **2014**, *2014*, 1-26.
(46) Ashby, PD, Olynick, DL, Ogletree, DF, Naulleau, PP, Resist Materials for Extreme Ultraviolet Lithography: Toward Low-Cost Single-Digit-Nanometer Patterning. *Adv Mater* **2015**, *27*, 5813-5819.
(47) Ravi Kiran, N, Chauhan, M, Sharma, SK, Ghosh, S, Gonsalves, KE, Resists for Helium Ion Beam Lithography: Recent Advances. *ACS Appl Electron Mater* **2020**, *2*, 3805-3817.
(48) Sazanovich, IV, Alamiry, MAH, Best, J, Bennett, RD, Bouganov, OV, Davies, ES, Grivin, VP, Meijer, AJHM, Plyusnin, VF, Ronayne, KL, Shelton, AH, Tikhomirov, SA, Towrie, M, Weinstein, JA, Excited State Dynamics of a Pt-Ii Diimine Complex Bearing a Naphthalene-Diimide Electron Acceptor. *Inorg Chem* **2008**, *47*, 10432-10445.
(49) Glik, EA, Kinayyigit, S, Ronayne, KL, Towrie, M, Sazanovich, IV, Weinstein, JA, Castellano, FN, Ultrafast Excited State Dynamics of Pt(II) Chromophores Bearing Multiple Infrared Absorbers. *Inorg Chem* **2008**, *47*, 6974-6983.
(50) Shao, Y, Molnar, LF, Jung, Y, Kussmann, J, Ochsenfeld, C, Brown, ST, Gilbert, AT, Slipchenko, LV, Levchenko, SV, O'Neill, DP, DiStasio, RJ, Lochan, RC, Wang, T, Beran, GJ, Besley, NA, Herbert, JM, Lin, CY, Van Voorhis, T, Chien, SH, Sodt, A, Steele, RP, Rassolov, VA, Maslen, PE, Korambath, PP, Adamson, RD, Austin, B, Baker, J, Byrd, EF, Dachsel, H, Doerksen, RJ, Dreuw, A, Dunietz, BD, Dutoi, AD, Furlani, TR, Gwaltney, SR, Heyden, A, Hirata, S, Hsu, CP, Kedziora, G, Khaliullin, RZ, Klunzinger, P, Lee, AM, Lee, MS, Liang, W, Lotan, I, Nair, N, Peters, B, Proynov, EI, Pieniazek, PA, Rhee, YM, Ritchie, J, Rosta, E, Sherrill, CD, Simmonett, AC, Subotnik, JE, Woodcock, HR, Zhang, W, Bell, AT, Chakraborty, AK, Chipman, DM, Keil, FJ, Warshel, A, Hehre, WJ, Schaefer, HR, Kong, J, Krylov, AI, Gill, PM, Head-Gordon, M, Advances in Methods and Algorithms in a Modern Quantum Chemistry Program Package. *Phys Chem Chem Phys* **2006**, *8*, 3172-91.